DYNAMIC APERTURE ESTIMATES AND PHASE SPACE DISTORTIONS IN NONLINEAR BETATRONIC MOTION

E. Todesco[*] and M. Giovannozzi

Abstract

Symplectic mappings which modelize the 4D betatronic motion in a magnetic lattice are considered. We define the dynamic aperture in terms of the connected volume in phase space of initial conditions which are bounded for a given number of iterations. Different methods for a fast estimate of this quantity are given; the analysis of the associated errors and the optimization of the integration steps are outlined. A comparison of the accuracy of these methods is given for both simple models and more realistic lattices.

Submitted to Phys. Rev. E

Geneva, Switzerland

November 29, 1995

1 INTRODUCTION

The presence of nonlinearities in the magnetic field of the elements of an accelerator can greatly reduce the stability domain, i.e., the region in phase space where one can safely operate with the beam [1], [2], [3]. An accurate estimate of the dimension of this domain, which is related to the so–called dynamic aperture, is crucial both for the understanding of the dynamics of existing machines [3] and for the specification of the lattice parameters of planned machines [4].

In this paper we restrict ourselves to the analysis of the nonlinear oscillations of the beam in the plane (x, y) transverse to the orbit (betatronic motion). Fixing a section of the machine, we analyse the dynamics in the four–dimensional phase space (x, p_x, y, p_y), p_x and p_y being the momenta associated to x and y.

The numerical estimate of the dynamic aperture is related to the computation of the volume in phase space of the initial conditions that are stable after a given number of revolutions around the machine. This set can be rather irregular, and it can have holes: in fact, initial conditions arbitrarily close to the origin can be unstable. This phenomenon, universally known as *Arnold diffusion* [5], occurs in systems whose phase space has dimension higher than two. Even if it is general belief that this effect is not of practical relevance for accelerator physics, it appears that it is difficult to give a rigorous definition of the dynamic aperture.

Moreover, the main difficulty in determining a reliable estimate of the stability domain for complicated lattices does not only stem from theoretical arguments. In fact, a numerical evaluation of the volume of the stable initial conditions is very CPU time consuming, as in principle one should scan the four variables (x, p_x, y, p_y).

To overcome these problems for complicated lattices, a pragmatic approach has been proposed [2] [3]: tracking is carried out over initial conditions with zero phases ($p_x = p_y = 0$) and a fixed ratio x/y (in most cases one uses $x/y = 1$), with a large gain in the CPU time. Unfortunately, this approach is not completely correct as it does not take into account two main effects, namely the distortion of the orbits along the phases and the different dynamics of the particles with various ratios x/y. The influence of the distortion along the phases can be evaluated through the *smear*. This quantity measures the standard deviation of the particle amplitude along the orbit [6]. Moreover, several studies have been performed to analyse the dynamics of particles with various ratios of x/y (see for instance [1] [3] [7]). Neglecting these effects, the computed dynamic aperture will be affected by errors which cannot be estimated a priori.

To find an efficient and correct way to estimate the dynamic aperture is the key point in problems like that of sorting the magnets according to their random magnetic errors [8]. In fact, as for all the optimization procedures, the analysis of the errors affecting the computation of the dynamic aperture is crucial to determine the validity of the correcting schemes. Furthermore, the study of the random errors requires to consider a rather large number of realizations of these

errors: the knowledge of the dependence of the accuracy on the integration steps allows one to choose the best compromise between CPU time and accuracy.

In this paper we present some original numerical methods to evaluate the dynamic aperture taking into account the phase space distortions. The first step in this analysis is to give a definition of dynamic aperture. We define it as the average distance in phase space of the border of stability, i.e. as the radius of the hypersphere whose volume is equal to the connected volume of stable initial conditions for a fixed number of iterations. Then we develop some algorithms for its evaluation. The direct implementation of the complete integration in phase space is very CPU time consuming: we show that in order to obtain a relative error of $1/(4J)$, one has to evaluate J^4 orbits using an optimized integration.

Indeed, we show that it is possible to exploit the dynamics to take into account the distortion of the orbits along the phases, thus avoiding the integration over these variables. As a result, the simulations are considerably faster, and one obtains an optimized relative error of the order of $1/(4J)$ by evaluating only J^2 orbits. We develop two algorithms to carry out these fast estimates: the first one is based on numerical integration [9], whilst the second one exploits the perturbative tools of normal forms [10] [11] [12].

We have carried out numerical simulations in order to check the effectiveness of our techniques, and to show that phase space distortions can be rather relevant. We analysed the Hénon map [12] [13], a LHC–like cell lattice with random errors [8], and a SPS lattice used for experiments [14]. All the computations were carried out for a short–term tracking (1000 turns). The results show that for the Hénon map and for the LHC–like cell lattice our estimates of the dynamic aperture are rather accurate (2%–3%). On the other hand, the results obtained by tracking particles with zero phases and satisfying $x/y = 1$ are by far less accurate (5%–15%). This is an indication of the fact that the phase space distortions are not negligible. In the case of the SPS lattice the situation is even worse due to the strong non linearities: the fast estimate along the line $x/y = 1$ is affected by a very strong error (15%–45%), whilst our methods are still reliable, even though the strong nonlinearities in the model reduce the accuracy with respect to the previous cases (6%–9%). The effect of long-term and of neglected ingredients (for instance, modulation due to ripple) can reduce the very strong phase space distortions found for the SPS model: we present the short term results in order to test the precision of the outlined methods in the situations where the distortion is higher.

The structure of the paper is the following: in section 2 we consider the 2D betatronic motion, which is propaedeutic to the analysis of the more realistic 4D case. In 2.1 we introduce the notations; in 2.2 we give a definition of dynamic aperture and in 2.3 the algorithms are presented. A detailed discussion of the error sources and of the implementation can be found in the Appendix A. In section 2.4 the numerical results are presented. The same structure is used for section 3, where the 4D case is analysed. Concluding remarks are given in

section 4.

2 2D betatronic motion

2.1 The model

We consider the transverse motion in a circular particle accelerator: let $\mathbf{F}$ be the one–turn map [10] [11] [12] which gives the position $\mathbf{x}_{n+1}$ of a single particle in phase space as a function of its position at the previous turn $\mathbf{x}_n$:

$$\mathbf{x}_{n+1} = \mathbf{F}(\mathbf{x}_n). \tag{1}$$

The iterates of the one–turn map are computed through the successive application of the maps of each element (tracking procedure). In this section we restrict ourselves to the analysis of the 2D betatronic motion, i.e. we have $\mathbf{x} = (x, p_x)$. We assume that x, p_x are the Courant–Snyder coordinates, so that the linear part of the map is a rotation by a constant angle $\omega = 2\pi\nu$. The parameter ν is the linear tune. The phase space of the map has a well known structure [5] [12]: around the origin, which is an elliptic fixed point, one has closed curves (1D KAM tori), and wherever the nonlinear tune satisfies a resonant condition, the invariant curves are broken into islands; when nonlinearities are dominant, one reaches a stability border beyond which a fast escape to infinity occurs.

The KAM tori separate different phase space domains, i.e. an initial condition inside a KAM torus cannot cross it: therefore, there exists a last connected invariant curve whose interior represents a set of stable initial conditions. Outside this curve, one can only have islands of stability, scattered in the sea of initial conditions which escape to infinity. In Fig. 1 we plot the phase portrait of the Hénon map [see Eq. (6), where the parameter μ is set to zero] whose linear frequency is $\nu = 0.28$. The last connected invariant curve is marked in boldface; one can also observe a chain of islands of period 15 outside the stable domain.

2.2 Dynamic aperture definition (2D case)

The stability domain of the one–turn map of Eq. (1) is given by the area of the set of initial conditions enclosed by the last connected stable invariant curve. We define the dynamic aperture as the radius of the circle whose area is equal to the area of the stability domain. We make the following remarks:

- Islands: The above definition excludes the islands of stability which are usually neglected in accelerator physics, since they are not a safe place where to inject the beam.

- Why phase space ? One has to consider the area in phase space $\mathbf{x} = (x, p_x)$ and not only the projection of this area on the physical space x. In fact, even though one is interested in the physical dimension of the allowed stable

4

domain for the beam, the betatronic motion exchanges the roles of x and p_x along the circumference of the machine.

- Long-term stability. The above definition is valid for infinite times; in fact, in accelerator physics, one is interested in stability over long but finite times, corresponding to the typical time of the experiment run. For a machine such as the planned LHC [4] this time is of the order of 10^8 turns, which is beyond the capability of modern computers: therefore, one usually considers short term stability (i.e. ≈ 1000 turns) as a first indication. More refined estimates can be obtained through medium–term tracking in conjunction with numerical tools such as Lyapunov exponents [15] or survival plots [16]. In the followings, we will always consider the dynamic aperture as a function of the number of iterates, without dealing with the relation between short-term and long-term stability.

2.3 Methods to compute the 2D dynamic aperture

- Method 1: direct integration. Let us define $\chi(x, p_x)$ as the characteristic function of the set of initial conditions which are bounded under N iterations [i.e. $\chi(x, p_x)$ is zero if the orbit with initial condition (x, p_x) is lost, and unity if it is stable after N iterations]. Then, the dynamic aperture is related to the area of this set in phase space:

$$\int \int \chi(x, p_x) \, dx \, dp_x. \tag{2}$$

Since the linear motion is a rotation by a constant angle, it is natural to use polar coordinates (r, ϑ):

$$\int_0^{2\pi} \int_0^\infty \chi(r \cos \vartheta, r \sin \vartheta) \, r \, dr \, d\vartheta. \tag{3}$$

Having fixed ϑ, let $r(\vartheta)$ be the distance along ϑ of the last connected invariant curve (i.e., the curve marked in boldface in Fig. 1). Then, we define the area of the stability domain as

$$A_\vartheta = \int_0^{2\pi} \int_0^{r(\vartheta)} r \, dr \, d\vartheta = \frac{1}{2} \int_0^{2\pi} r(\vartheta)^2 d\vartheta. \tag{4}$$

In this way, one neglects the contribution given by the stable islands outside the last connected invariant curve. The subscript indicates that an average over the angle ϑ is carried out. The details of the implementation of this approach are given in Appendix A.1.

Indeed, once the last stable invariant curve is found for a given direction $\overline{\vartheta}$, one already knows the whole orbit through numerical iteration. This implies that the scan in the initial conditions over the angle can be avoided

5

if one can evaluate the area of the orbit (i.e. the nonlinear invariant), given the N iterates. We will describe two different approaches which provide an estimate of the invariant of motion. Hence one can avoid to scan the angle ϑ with a substantial reduction of the CPU time.

- Method 2: integration over the dynamics. In this case, we fix an angle $\overline{\vartheta}$, and we define $r(\overline{\vartheta})$ as in Method 1. We evaluate N iterates of the orbit with initial condition $(r(\overline{\vartheta})\cos\overline{\vartheta}, r(\overline{\vartheta})\sin\overline{\vartheta})$; let $r^{(n)}(\overline{\vartheta})$ and $\vartheta^{(n)}(\overline{\vartheta})$ be the amplitudes and the phases of the n–th iterate. In order to estimate the area of the last stable curve, one can replace the average of r^2 over the angle [see Eq. (4)] with the average over the iterates (namely we are replacing a space average with a time average):

$$\frac{1}{2\pi}\int_0^{2\pi} r^2(\vartheta)\,d\vartheta \longrightarrow \lim_{N\to\infty}\frac{1}{N}\sum_{n=1}^{N}[r^{(n)}(\overline{\vartheta})]^2. \tag{5}$$

The dependence of the r.h.s. on the choice of $\overline{\vartheta}$ is very weak, since every $\overline{\vartheta}$ should approximate the same orbit provided the integration step in r is small enough. Nevertheless, in order to carry out the substitution (5), one has to assume the following hypotheses.

- The frequency of the last invariant curve is irrational, i.e. the iterates are dense on the last invariant orbit.
- The invariant measure associated to the dynamics over the last stable curve is uniform, i.e. the distribution of the phases of the iterates on the last invariant curve is constant.

In Fig. 2 we plot the distribution of the phases of 50000 iterates of the last stable curve of the Hénon map at $\nu = 0.28$. One can see that, even if the iterates are dense on the angular interval $[0, 2\pi]$ (i.e., there are no gaps), the distribution is far from being uniform. This effect is well known [5] [12]: close to hyperbolic (i.e. unstable) fixed points, which arise from nonlinear resonances, the motion can be very slow, and therefore the distribution of the iterates over the invariant curve can be significantly non uniform. In fact, the four major peaks in Fig. 2 correspond to the four hyperbolic fixed points which lie outside the stability domain (see Fig. 1). In order to cure this effect one has to carefully consider the information folded in the dynamics [9]. In Appendix A.2 we give the details of this method; the obtained dynamic aperture estimate is denoted by r_d.

- Method 3: normal forms. The normal forms series allow one to give an analytic approximation of the orbit in phase space, and therefore provide another method to estimate the dynamic aperture. According to the nonresonant normal form theory, one conjugates the map $\mathbf{F}$ with a normal form $\mathbf{U}$, which is an amplitude–dependent rotation, using a conjugating function $\mathbf{\Phi}$ (see Ref. [10] [11] and [12]). The orbits of $\mathbf{F}$ are transformed through the

inverse conjugating function $\boldsymbol{\Psi} = \boldsymbol{\Phi}^{-1}$ to circles in the normalized plane. Since $\boldsymbol{\Psi}$ is area–preserving, the area of the last stable orbit (i.e. the dynamic aperture) can be evaluated by taking π times the radius of the orbit transformed in the normalized space. In Appendix A.3 we give the details of the implementation of this algorithm; the obtained dynamic aperture estimate is denoted by r_{nf}.

2.4 Numerical results

We consider a lattice model made up of a linear part plus a nonlinear element containing a sextupole and an octupole in the one–kick approximation:

$$\begin{cases} x' = \cos(2\pi\nu_x)x + \sin(2\pi\nu_x)(p_x + x^2 + \mu x^3) \\ \\ p'_x = -\sin(2\pi\nu_x)x + \cos(2\pi\nu_x)(p_x + x^2 + \mu x^3), \end{cases} \tag{6}$$

where μ can be expressed as

$$\mu = \frac{1}{3}\frac{K_3}{K_2}\sqrt{\beta}. \tag{7}$$

The quantities K_2, K_3 represent the integrated sextupolar and octupolar gradient respectively, whilst β is the value of the beta function in the nonlinear element.

When $\mu = 0$ one obtains the conservative Hénon map [12]. We computed the dynamic aperture over $N = 1000$ turns for different values of the parameter μ, having set the tune to the value $\nu_x = 0.28$. In Table 1 we show the dynamic apertures evaluated using the described methods (i.e., r_ϑ, r_d and r_{nf}); moreover we give the minimum r_{min} and the maximum r_{max} distance of the last invariant curve from the origin, and its intersection r_0 with the positive x axes. We used r_ϑ computed with 100 steps for each variable as the exact dynamic aperture: indeed, this estimate is affected by a relative error of the order of 1%; we verified the validity of the error bound by varying the number of integration steps and checking the stability of the computed dynamic aperture within the error. In the last row of Table 1 the average relative error of r_0, r_d, r_{nf} with respect to r_θ is given.

In all the numerical simulations, the number of steps in r was 100; r_d was computed over 100 iterates, and the normal form estimate r_{nf} was evaluated using a truncation order between 3 and 8, choosing the order which minimizes the error provided by the composition of the conjugating functions $\boldsymbol{\Phi}$ and $\boldsymbol{\Psi}$.

In all the cases considered, there is a wide distortion of the phase space, and therefore r_0 is a bad estimate of the stability area in phase space. Nevertheless, both r_d and r_{nf} can provide rather accurate estimates of the dynamic aperture without making the scan over the angle.

3 4D betatronic motion

3.1 The model

We analyze a 4D symplectic mapping, which can be written as

$$\mathbf{x}' = \mathbf{F}(\mathbf{x}) \qquad \mathbf{x} = (x, p_x, y, p_y) \tag{8}$$

where $\mathbf{x}$ is now a vector in the 4D euclidean phase space. The linear motion is given by the direct product of two constant rotations in the planes (x, p_x) and (y, p_y) by the linear tunes ν_1 and ν_2.

3.2 Dynamic aperture definition (4D case)

Let us consider the phase space volume of the initial conditions which are bounded after N iterations:

$$\int \int \int \int \chi(x, p_x, y, p_y) \, dx \, dp_x \, dy \, dp_y, \tag{9}$$

where $\chi(x, p_x, y, py)$ is the generalization of the characteristic function [see Eq. (2)] to the 4D case. Since in 4D the invariant curves (i.e. 2D KAM tori) do not separate different domains of phase space, the concept of last invariant curve (which surrounds stable initial conditions) is not valid anymore [5] [12]. In principle, the stability domain for a fixed number of iterations could be a rather peculiar set in phase space, with holes and very irregular structures. However, it seems from numerical simulations [2] [3] [7] [8] [16] that these situations are not typical of weakly nonlinear lattices, where these structures have no practical relevance, since they occupy a negligible fraction of the phase space volume. Therefore, in general, there exists a connected region of initial conditions which are stable for a given number of iterations.

3.3 Methods to compute the 4D dynamic aperture

In this section we will generalize the methods already presented for the two–dimensional case (again the details can be found in the Appendix 2).

- Method 1: direct integration. In order to exclude the disconnected part of the stability domain in the integral (9), we have to choose a suitable coordinate transformation. Since the linear motion is the direct product of constant rotations, the natural choice is to use polar variables $(r_1, \vartheta_1, r_2, \vartheta_2)$: r_1 and r_2 are the linear invariants. The nonlinear part of the equations of motion adds a coupling between the two planes, the perturbative parameter being the distance to the origin. Therefore it is natural to replace r_1 and r_2

with the polar variables $r \cos \alpha$ and $r \sin \alpha$:

$$
\begin{cases}
x & = & r \cos \alpha \cos \vartheta_1 \\[1em]
p_x & = & r \cos \alpha \sin \vartheta_1 \qquad & r \in [0, +\infty[\\[0.3em]
& & & \vartheta_1, \vartheta_2 \in [0, 2\pi[\\[0.3em]
y & = & r \sin \alpha \cos \vartheta_2 & \alpha \in [0, \pi/2] \\[1em]
p_y & = & r \sin \alpha \sin \vartheta_2 ;
\end{cases}
\tag{10}
$$

substituting in Eq. (9) we obtain

$$
\int_0^{2\pi} \int_0^{2\pi} \int_0^{\pi/2} \int_0^{\infty} \chi(r, \alpha, \vartheta_1, \vartheta_2) \, r^3 \sin(\alpha) \cos(\alpha) \, dr \, d\alpha \, d\vartheta_1 \, d\vartheta_2 . \tag{11}
$$

Having fixed α, ϑ_1 and ϑ_2, let $r(\alpha, \vartheta_1, \vartheta_2)$ be the first value of r whose orbit is not bounded after N iterations. Then, the area of a connected stability domain is

$$
A_{\alpha, \vartheta_1, \vartheta_2} = \frac{1}{8} \int_0^{2\pi} \int_0^{2\pi} \int_0^{\pi/2} [r(\alpha, \vartheta_1, \vartheta_2)]^4 \sin(2\alpha) \, d\alpha \, d\vartheta_1 \, d\vartheta_2 . \tag{12}
$$

In this way one excludes stable islands which are not connected to the main stable domain. In principle, this method can lead to also exclude connected parts. We define the dynamic aperture as the radius of the hypersphere that has the same volume as the stability domain:

$$
r_{\alpha, \vartheta_1, \vartheta_2} = \left(\frac{2 A_{\alpha, \vartheta_1, \vartheta_2}}{\pi^2} \right)^{1/4} . \tag{13}
$$

- <u>Method 2: integration over the dynamics.</u> The generalization of Method 2 to the 4D case is straightforward and it will be discussed in Appendix 2.2; the obtained dynamic aperture estimate is denoted by $r_{\alpha, d}$.

- <u>Method 3: normal forms.</u> According to the nonresonant normal form theory, using a conjugating function $\boldsymbol{\Phi}$ one transforms a 4D map $\mathbf{F}$ into its normal form $\mathbf{U}$ [11] [12] [8]. The normal form is a direct product of rotations in the two phase planes (x, p_x) and (y, p_y), whose nonlinear frequencies depend on the distance to the origin. The two components of the inverse conjugating function Ψ_1 and Ψ_2 give the approximated nonlinear invariants ρ_1 and ρ_2. Again $r(\alpha, \overline{\vartheta}_1, \overline{\vartheta}_2)$ stands for the first value of the radial coordinate for which a particle loss occurs along the direction $\alpha, \overline{\vartheta}_1, \overline{\vartheta}_2$, then, thanks to the properties of the normal forms, the nonlinear invariants ρ_1, ρ_2 will be independent on the values of the phases $\overline{\vartheta}_1, \overline{\vartheta}_2$. Therefore in Eq. 12 the integration over the phases can be trivially computed, and the final result will be

$$
A_{\alpha, nf} = \frac{\pi^2}{2} \int_0^{\pi/2} [\rho_1(r, \alpha) + \rho_2(r, \alpha)]^2 \sin(2\alpha) \, d\alpha \tag{14}
$$

The details of the implementation of this approach are given in Appendix 2.3; the obtained dynamic aperture estimate is denote by $r_{\alpha, nf}$.

9

3.4 Numerical results: sextupole and octupole kick

We have considered a lattice made up of a linear part plus a nonlinear element containing a sextupole and an octupole in the one–kick approximation: the one–turn map reads

$$
\begin{cases}
x' &= \cos(2\pi\nu_x)x + \sin(2\pi\nu_x)[p_x + (x^2 - y^2) + \mu(x^3 - 3xy^2)] \\[2mm]
p_x' &= -\sin(2\pi\nu_x)x + \cos(2\pi\nu_x)[p_x + (x^2 - y^2) + \mu(x^3 - 3xy^2)] \\[2mm]
y' &= \cos(2\pi\nu_y)y + \sin(2\pi\nu_y)[p_y - 2xy + \mu(3x^2y - y^3)] \\[2mm]
p_y' &= -\sin(2\pi\nu_y)y + \cos(2\pi\nu_y)[p_y - 2xy + \mu(3x^2y - y^3)]
\end{cases}
\tag{15}
$$

As for the 2D model (6), the parameter μ represents the ratio between the sextupolar and octupolar integrated gradients. When $\mu = 0$ one recovers the 4D conservative Hénon map [12].

As a first step in our analysis, we have carried out numerical experiments using the previous model in order to illustrate some pathological situations which can occur when one tries to estimate the dynamic aperture in 4D.

Let us define the stability diagram as the set of the initial conditions $(x, 0, y, 0)$ which are bounded after N iterations: this corresponds to make a scan over r and α, fixing the phases ϑ_1 and ϑ_2 to zero [see Eq. (13)]. In Fig. 3 we show the stability diagram for the map given in Eq. (15), with $\mu = -0.2$ and close to the resonance [4,0], namely $\nu_x = 0.25$ and $\nu_y = 0.61803$; 1000 iterations were considered. One can observe that the shaded area is very irregular, with tiny holes well inside the stability domain: the definition of dynamic aperture proposed in Sec. 3.3, leads to an underestimation of the actual dynamic aperture. Indeed, if one examines the same stability domain at a higher number of iterations (see Fig. 4, where 50000 iterations are considered), it turns out that it is not obvious to define the dynamic aperture for this case. On the other hand, when we are far from low order resonances, the situation seems to be, in general, more regular: in Fig. 5 we plot the stability diagram of the map (15) with $\mu = 1$ and $\nu_x = 0.28$ and $\nu_y = 0.31$. The stability domain is full, and its border is more regular.

We stress that in the rest of the computations, 1000 iterations were considered. We computed the dynamic aperture over $N = 1000$ turns for different values of the parameter μ, setting the tunes to the LHC values $\nu_x = 0.28$, $\nu_y = 0.31$. In Table 2 we give the minimum and maximum distance to the origin of the stability border r_{min} and r_{max}, and the dynamic apertures $r_{\alpha,\vartheta_1,\vartheta_2}$, $r_{\alpha,d}$ and $r_{\alpha,nf}$ evaluated using the three definitions given in Appendix 2. Moreover, we also give the position r_0 of the last invariant curve along the direction $\alpha = \pi/4$ (i.e. equal invariants), and $\vartheta_1 = \vartheta_2 = 0$; this is the indicator which is commonly used for fast dynamic aperture estimates

of complicated lattices [2] [3]. In the last row we quote the average relative errors with respect to $r_{\alpha,\vartheta_1,\vartheta_2}$ computed with 20 steps for each variable: this dynamic aperture estimate is affected by a relative error of the order of 2%; also in this case, we verified the validity of the error bound by varying the number of integration steps and checking the stability of the computed dynamic aperture within the error. For the methods which avoid the integration over the phases, the number of steps in α and in r is 20; $r_{\alpha,d}$ is computed over 1000 iterates. The normal form truncation is carried with the same criteria used for the 2D case.

Both the normal form and the average over the dynamics give very good estimates. Although the evaluation of the dynamic aperture along the bisetrix r_0 is more precise than in the 2D case, it is affected by an average error of 6%.

3.5   Numerical results: LHC cell lattice with random errors

We consider a lattice made up of 8 LHC–like cells [4] plus a phase shifter to set the linear tunes to the values $\nu_x = 0.28$, $\nu_y = 0.31$. Two different sets of nonlinearities have been considered:

- A lattice with only random sextupolar components in the dipoles.
- A lattice with random sextupolar, octupolar and decapolar components in the dipoles.

The multipolar gradients have been set to the estimated values of the LHC dipole errors. For each case we analysed 10 different seeds. In Table 3 we report the relative errors between Methods 2, 3, and Method 1. The same values of the number of steps as in the previous 4D model have been used. The results confirm the trend of the data shown in Table 2: both $r_{\alpha,d}$ and $r_{\alpha,nf}$ provide an estimate of the dynamic aperture which is in agreement with the direct integration of the stability domain, without making the scan over two angles ϑ_1 and ϑ_2. The fast dynamic aperture estimate r_0 (carried along one direction in phase space) neglects both the distortion of the orbit and the contributions coming from particles with different emittances: these phenomena are relevant, and thus make this estimate rather imprecise.

3.6   Numerical results: SPS

Finally, we consider the SPS lattice corresponding to the set–up used for nonlinear dynamics experiments [14]. The nonlinear part of the lattice is made up by 8 strong extraction sextupoles, and by 108 chromatic sextupoles. Two working points have been considered: the first one (WP1) at $\nu_x = 26.637$ and $\nu_y = 26.533$, which is close to resonances of order 7 and 8; the second one (WP2) is $\nu_y = 26.605$ and $\nu_y = 26.538$, which is close to

11

resonances of order 5. Both working points correspond to very perturbed situations where the nonlinear resonances are excited and the phase space is strongly deformed. In Fig. 6 we plot the stability diagrams previously defined in section 3.4 of WP1 and WP2 respectively. The dependence of the stability domain on the ratio of the invariants is extremely irregular. In Table 3 the different estimates of the dynamic aperture r_0, $r_{\alpha,d}$ and $r_{\alpha,nf}$ are compared to the estimate $r_{\alpha,\vartheta_1,\vartheta_2}$ computed with 20 steps in each variable. The results show that, due to the high distortion in phase space, the estimate r_0, obtained on the line $x/y = 1$ is really imprecise (15%–40%). On the other hand, Methods 2 and 3 provide a better estimate, even if the error (5%–9%) is considerably higher than in the other cases; this is probably due to the strong nonlinearities of these models, which make the constants that were neglected in the error estimates considerably greater than one.

4   CPU time and dynamic aperture estimate

Up to now we focused our analysis on the accuracy of the methods proposed to estimate the dynamic aperture. From the discussion of the different methods, it should be clear, however, that they differ not only for the accuracy, but also for the CPU time. In Table 4, we present a summary of the computation time needed for the analysis of the LHC cell lattice and the SPS lattice. The simulations have been carried out on the CERN PARC system, which is a cluster of IBM RISC stations [17].

From Table 4 it is apparent the enormous gain obtained by evaluating the dynamic aperture along a line $x/y = 1$ with respect to the direct integration (by a factor $approx 10^5$ with the chosen integration steps). On the other hand, from the previous discussion, we know that this method can be rather imprecise. Methods 2 and 3 are almost equivalent as far as the CPU time requirement is concerned: they are slower than r_0 (by a factor $approx 20$), but their precision is considerably higher; moreover, they still provide a very large gain (≈ 400) with respect to direct integration. These CPU time are in very good agreement with the analytical estimates.

5   CONCLUDING REMARKS

In this paper we have discussed a definition of dynamic aperture of 2D and 4D betatronic motion when the effect of phase space distortions is not negligible. The basic reasons which do not allow a rigorous definition of this quantity as in the 2D case have been briefly reviewed. Three methods to compute the dynamic aperture and to estimate the associated errors have been presented. The optimization of the integration steps have been discussed as well. The straightforward implementation of the dynamic aperture

(Method 1) is very CPU time consuming: for this reason we have defined two alternative strategies (Method 2 and 3) that allow to avoid to scan over the angles in the phase planes. Both methods have given good results. Simulations carried out on simplified and more realistic models have shown that both the dependence on the phases and on the ratio of emittances can be crucial for obtaining a precise estimate. Since these numerical results are strongly model–dependent, we believe that for each model one should carefully test the relevance of these effects. In this way one can choose the most favorable combination of methods and therefore achieve the best compromise between accuracy and CPU time needed for the computations.

6 ACKNOWLEDGEMENTS

A Methods to compute the dynamic aperture (2D case)

A.1 Method 1: direct integration

To compute the dynamic aperture by performing the direct integration it is necessary to evaluate the Eq. (4). This requires the discretization of the angular and radial variables. When this formula is implemented on a computer code, one performs a scan over L angles $\vartheta_l = 2\pi l/L$ with $l = 1, ..., L$, and J radii $r_j = jR/J$, with $j = 1, ..., J$ (where R is the maximum of $r(\vartheta_l)$ over l), hence the area of the stability domain A_ϑ and the related dynamic aperture r_ϑ read

$$r_\vartheta = \sqrt{\frac{A_\vartheta}{\pi}} = \sqrt{\frac{1}{L} \sum_{l=1}^{L} [r(\vartheta_l)]^2} \qquad \text{where} \qquad r(\vartheta_l)\frac{J}{R} \in \mathbf{N}. \qquad (16)$$

The somewhat strange condition $r(\vartheta_l)J/R \in \mathbf{N}$ means that the radial variable is discretized and it is a multiple of the step R.

Error sources. The discretization both in the angular and in the radial variables leads to an integration error, which can be estimated using the standard tools of numerical analysis.

– The discretization in the angle ϑ corresponds to a trapezoidal rule of integration: depending on the regularity of the curve $r(\vartheta)$, one can have different estimates [18]. If the derivative of $r(\vartheta)$ is bounded, then the relative error on the area A_ϑ is proportional to the inverse of the number of steps L^{-1}; in case the derivative is more regular, the estimate L^{-2} holds. Since we are at the edge of the stability domain, the curve $r = r(\vartheta)$ can be rather irregular. Therefore, in the followings we will always assume that the more pessimistic estimate L^{-1} holds.

– The discretization in the radius r gives a relative error proportional to the inverse of the number of steps in the amplitude J^{-1}.

Step optimization. One should choose integration steps that produce comparable errors, i.e. $J \propto L$. In this way, neglecting the constants which are in front of the error estimates, one can obtain a relative error in r_ϑ of $1/(2J)$ by evaluating J^2 orbits, i.e. $J^2 N$ iterates [1].

A.2 Method 2: integration over the dynamics

As already mentioned, the distribution of the phases is usually highly non uniform. For this reason a space average cannot be simply replaced by a time average [see Eq. 5]. In order to cure this effect one can use the following approach:

– We fix $\overline{\vartheta}$, and we find $r(\overline{\vartheta})$ as in Method 1, computing the N iterates of the orbit.

– We divide $[0, 2\pi[$ in M equal intervals (with $M \leq N$), such that each interval contains at least the phase of one iterate of the orbit.

– For each interval $m = 1, ..., M$ we compute r_m, which is the average distance of the iterates whose phase falls in that interval.

– Finally, the dynamic aperture is computed as

$$r_d = \sqrt{\frac{1}{M} \sum_{m=1}^{M} [r_m]^2}. \tag{17}$$

We denote this definition[2] by the label d.

The number of intervals M should be as high as possible (having fixed the number of iterates N) in order to minimize the integration error.

Error sources. The error is given by the following contributions.

---

[1] The factor 2 in the error estimate of r_ϑ is due to the square root in Eq. (16), i.e. to the phase space dimension.

[2] Actually, one can define more refined methods to estimate the invariant when the motion is weakly perturbed [19] and obtain better estimates of the accuracy. Since we are at the edge of the stability domain, we believe that these methods do not provide a significant gain with respect to the outlined procedure.

– Discretization in the angle ϑ: the relative error is proportional to M^{-1}.
– Discretization in the radius r: the relative error is proportional to the inverse of the number of steps J^{-1}.

Step optimization. Also in this case one should choose integration steps that produce comparable errors, i.e. $J \propto M$. In this way, if the constants in front of the error estimates are neglected, one obtains a relative error in r_d of $1/(2J)$ by evaluating J orbits, i.e. JN iterates. Therefore one obtains the same relative error than with Method 1 but with JN iterations instead of J^2N.

A.3   Method 3: normal forms

The dynamic aperture can also be estimated by using normal forms, since they allow to quantify the nonlinear invariant (i.e. the area of the last stable curve). We summarize the method in the following steps:

– We fix $\overline{\vartheta}$, and compute $r(\overline{\vartheta})$.
– We compute the value of the invariant through the truncated inverse conjugating function $\boldsymbol{\Psi}$

$$\rho(\overline{\vartheta}) = |\boldsymbol{\Psi}(r(\overline{\vartheta})\cos\overline{\vartheta}, r(\overline{\vartheta})\sin\overline{\vartheta})|^2 : \tag{18}$$

this value is independent of $\overline{\vartheta}$ up to a given precision, which is the approximation provided by the normal form to the dynamics of the map $\mathbf{F}$.
– The area of the stable domain A_{nf} and the related dynamic aperture r_{nf} is given by

$$r_{nf} = \sqrt{\frac{A_{nf}}{\pi}} = \sqrt{\rho(\overline{\vartheta})}. \tag{19}$$

Error sources. The error is given by the following contributions.

– Discretization in the radius r (J steps), which leads to a relative error in the dynamic aperture estimate proportional to J^{-1}.
– Normal form error. The application of normal forms close to the dynamic aperture can give inaccurate results [12] [20]. The normal form error is due to the divergence of the perturbative series and to the truncation of the series which, in turns, leads to neglect the higher orders contributions. If the linear frequencies are close to low resonances, the divergence appears at low truncation orders, and therefore one is forced to compute the perturbative series at low orders, neglecting higher orders contribution which can be relevant. In the numerical examples analyzed in this paper, the linear frequencies are far from low order resonances, such as in real accelerators, and therefore the normal forms turn out to be very accurate.

2 Methods to compute the dynamic aperture (4D case)

2.1 Method 1: direct integration

When Eq. (12) is implemented on a computer code, one considers K steps in the angle α and L steps in the angles ϑ_1, ϑ_2: the dynamic aperture reads

$$r_{\alpha,\vartheta_1,\vartheta_2} = \left(\frac{\pi}{2KL^2} \sum_{k=1}^{K} \sum_{l_1=1}^{L} \sum_{l_2=1}^{L} [r(\alpha_k, \vartheta_{1l_1}, \vartheta_{2l_2})]^4 \sin(2\alpha_k) \right)^{1/4}, \qquad (20)$$

and the discretization condition over the radius r reads

$$r(\alpha_k, \vartheta_{1l_1}, \vartheta_{2l_2}) \frac{J}{R} \in \mathbf{N}. \qquad (21)$$

<u>Error sources</u>. The error is given by the following contributions.

- The discretization in the angles ϑ_1 and ϑ_2 gives a relative error proportional to L^{-1} (see the analysis of the 2D case).

- The discretization in the angle α gives a relative error proportional to K^{-1}.

- The discretization in the radius r gives a relative error proportional to J^{-1}.

<u>Step optimization</u>. One should choose integration steps which produce comparable errors, i.e. $J \propto K \propto L$. In this way, neglecting the constants which are in front of the error estimates, one can obtain a relative error of $1/(4J)$ by evaluating J^4 orbits, i.e. NJ^4 iterates[3]. The fourth power in the number of orbits comes from the dimensionality of phase space, and makes a precise estimate of the dynamic aperture very CPU time consuming: for instance, a 2.5% precision is obtained with $J = 10$, which implies the evaluation of 10 000 orbits. Nevertheless, also in this case one can develop some methods to avoid the integration over ϑ_1 and ϑ_2.

2.2 Method 2: integration over the dynamics

The generalization of Method 2 to the 4D case is straightforward:

- We fix $\overline{\vartheta}_1$ and $\overline{\vartheta}_2$. We scan over α and we find the radius $r(\alpha, \overline{\vartheta}_1, \overline{\vartheta}_2)$, computing the N iterates of the orbit.

- We divide $[0, 2\pi[\times [0, 2\pi[$ in M^2 equal squares (with $M^2 \leq N$), such that each square contains at least the phase of one iterate of the last stable curve.

- For each square (m_1, m_2), where $m_1 = 1, ..., M$ and $m_2 = 1, ..., M$, we compute $r_{m_1, m_2}(\alpha, \overline{\vartheta}_1, \overline{\vartheta}_2)$, that is the average distance to the origin of the iterates which fall in that angular square.

---

[3]Also in this case, the factor 4 in the error estimate is due to the dimensionality of the phase space

- Finally, the dynamic aperture is computed as

$$r_{\alpha,d} = \left(\frac{\pi}{2KM^2} \sum_{m_1,m_2=1}^{M} \sum_{k=1}^{K} [r_{m_1,m_2}(\alpha_k, \overline{\vartheta}_1, \overline{\vartheta}_2)]^4 \sin(2\alpha_k) \right)^{1/4}. \qquad (22)$$

Error sources. The error is given by the following contributions.

- The discretization in the angles ϑ_1, ϑ_2, which is given by the M^2 squares over which the integration is carried out. The relative error in the dynamic aperture is proportional to $M^{-1} \propto N^{-1/2}$.

- Discretization in the angle α: the relative error is proportional to K^{-1}.

- Discretization in the radius r: the relative error is proportional to J^{-1}.

Step optimization. One should choose $J \propto K \propto \sqrt{M}$. Neglecting the multiplicative constants in the estimates, one can obtain a relative error of $1/(4J)$ evaluating J^2 orbits, i.e. $J^2 M^2 \propto J^2 N$ iterates: one saves a factor J^2 with respect to direct integration.

2.3 Method 3: normal forms

The dynamic aperture estimate based on normal forms tools is computed in the following way.

- We fix $\overline{\vartheta}_1$ and $\overline{\vartheta}_2$. We scan over α and we find the radius $r(\alpha, \overline{\vartheta}_1, \overline{\vartheta}_2)$ as in Method 2.

- We apply the inverse conjugating functions to the initial condition of the last stable curves to compute the nonlinear invariants:

$$\rho_1(\alpha, \overline{\vartheta}_1, \overline{\vartheta}_2) = \left| \Psi_1(r\cos\alpha\cos\overline{\vartheta}_1, r\cos\alpha\sin\overline{\vartheta}_1, r\sin\alpha\cos\overline{\vartheta}_2, r\sin\alpha\sin\overline{\vartheta}_2) \right|^2$$
$$\rho_2(\alpha, \overline{\vartheta}_1, \overline{\vartheta}_2) = \left| \Psi_2(r\cos\alpha\cos\overline{\vartheta}_1, r\cos\alpha\sin\overline{\vartheta}_1, r\sin\alpha\cos\overline{\vartheta}_2, r\sin\alpha\sin\overline{\vartheta}_2) \right|^2$$

$$(23)$$

- Then, the dynamic aperture reads

$$r_{\alpha,nf} = \left(\frac{\pi}{2K} \sum_{k=1}^{K} \{\rho_1(\alpha_k, \overline{\vartheta}_1, \overline{\vartheta}_2) + \rho_2(\alpha_k, \overline{\vartheta}_1, \overline{\vartheta}_2)\}^2 \sin(2\alpha_k) \right)^{1/4}. \qquad (24)$$

Error sources. The error is given by the following contributions.

- Discretization in the angle α: the relative error is proportional to K^{-1}.

- Discretization in the radius r: the relative error is proportional to J^{-1}.

- Normal form error. The same observations made for the 2D case are valid for the 4D.

17

Step optimization. One should choose $J \propto K$. Neglecting the multiplicative constants in the estimate, and assuming that the normal form error is smaller than the integration error over r and α, one obtains a relative error of $1/(4J)$ by evaluating J^2 orbits, i.e. J^2N iterates: one saves a factor J^2 with respect to direct integration (without constraints over the number of iterates such as in Method 2).

References

[1] F. Willeke, in *CERN Accelerator School 90–04*, edited by S. Turner (CERN, Geneva, 1990) pp. 156–183.

[2] W. Scandale, in *Third European Particle Accelerator Conference*, edited by H. Henke (Edition Frontiéres, Gif sur Yvette, 1993) pp. 264–268.

[3] F. Zimmermann, in *Fourth European Particle Accelerator Conference*, edited by V. Sueller et al. (World Scientific, Singapore, 1995) pp. 327–331.

[4] The LHC study group, CERN **91–03** (1991).

[5] J. D. Meiss, Rev. Mod. Phys. **64**, 795–848 (1992).

[6] N. Merminga, in *IEEE Conference series*, edited by F. Bennett and J. Kopta (IEEE, New York, 1990) pp. 1286–1288.

[7] F. Galluccio and W. Scandale, CERN SL (AP) **89–51** (1989).

[8] M. Giovannozzi, R. Grassi, W. Scandale and E. Todesco, Phys. Rev. E **52**, in press (1995).

[9] R. Brinkmann and F. Willeke, DESY **86–079** (1986).

[10] A. Bazzani, P. Mazzanti, G. Servizi and G. Turchetti, Nuovo Cim., B **102**, 51–80 (1988).

[11] E. Forest, M. Berz and J. Irwin, Part. Accel. **24**, 91–113 (1989).

[12] A. Bazzani, E. Todesco, G. Turchetti and G. Servizi, CERN **94–02** (1994).

[13] M. Hénon, Q. Appl. Math. **27**, 291–312 (1969).

[14] J. Gareyte, W. Scandale and F. Schmidt, in *Nonlinear Problems in Accelerator Physics*, edited by M. Berz et al (Institute of Physics Conference Series 131, Bristol, 1992) pp. 235–48.

[15] F. Schmidt, F. Willeke and F. Zimmermann, Part. Accel. **35**, 249–256 (1991).

[16] F. Galluccio and F. Schmidt, in *Third European Particle Accelerator Conference*, edited by H. Henke (Edition Frontiéres, Gif sur Yvette, 1993) pp. 640–642.

[17] T. Bell et al., CERN CN **94–8** (1994).

[18] J. Stoer, Introduction to numerical analysis (Springer, New York, 1980).

[19] R. L. Warnock and R. D. Ruth, Physica D **56**, 188 (1992).

[20] G. Turchetti, in *Number theory and physics*, edited by J. M. Luck and P. Moussa (Springer Verlag, Berlin–Heidelberg, 1990) pp. 223–34.

Table 1: Dynamic aperture estimates for the 2D model.

μ	r_{min}	r_{max}	r_0	r_ϑ	r_d	r_{nf}
-1	0.49	0.89	0.504	0.611	0.590	0.586
0	0.61	1.19	0.630	0.716	0.717	0.706
1	0.57	1.13	0.679	0.769	0.739	0.712
10	0.15	0.20	0.168	0.167	0.167	0.167
Average Relative Error			10%	–	2%	3%

Table 2: Dynamic aperture estimates for the 4D model.

μ	r_{min}	r_{max}	r_0	$r_{\alpha,\vartheta_1,\vartheta_2}$	$r_{\alpha,d}$	$r_{\alpha,nf}$
-1	0.24	0.53	0.392	0.356	0.375	0.371
0	0.29	0.77	0.371	0.380	0.392	0.378
1	0.30	0.66	0.405	0.430	0.432	0.430
10	0.12	0.25	0.177	0.166	0.161	0.169
Average Relative Error			6%	–	3%	2%

Table 3: Dynamic aperture estimates for the LHC and SPS lattices.

Model	Average Relative Error w.r.t. $r_{\alpha,\theta_1,\theta_2}$		
	r_0	$r_{\alpha,d}$	$r_{\alpha,nf}$
LHC - Sex. only	16%	2%	3%
LHC - All mult.	9%	1.5%	2%
SPS - WP1	13%	9%	8%
SPS - WP2	37%	5%	6%

Table 4: CPU time for dynamic aperture estimates for the LHC and SPS lattices.

Model	Average CPU time (s)			
	$r_{\alpha,\theta_1,\theta_2}$	r_0	$r_{\alpha,d}$	$r_{\alpha,nf}$
LHC - Sex. only	13567	1	23	26
LHC - All mult.	13710	2	30	59
SPS - WP1	92280	14	271	263
SPS - WP2	101512	9	278	280
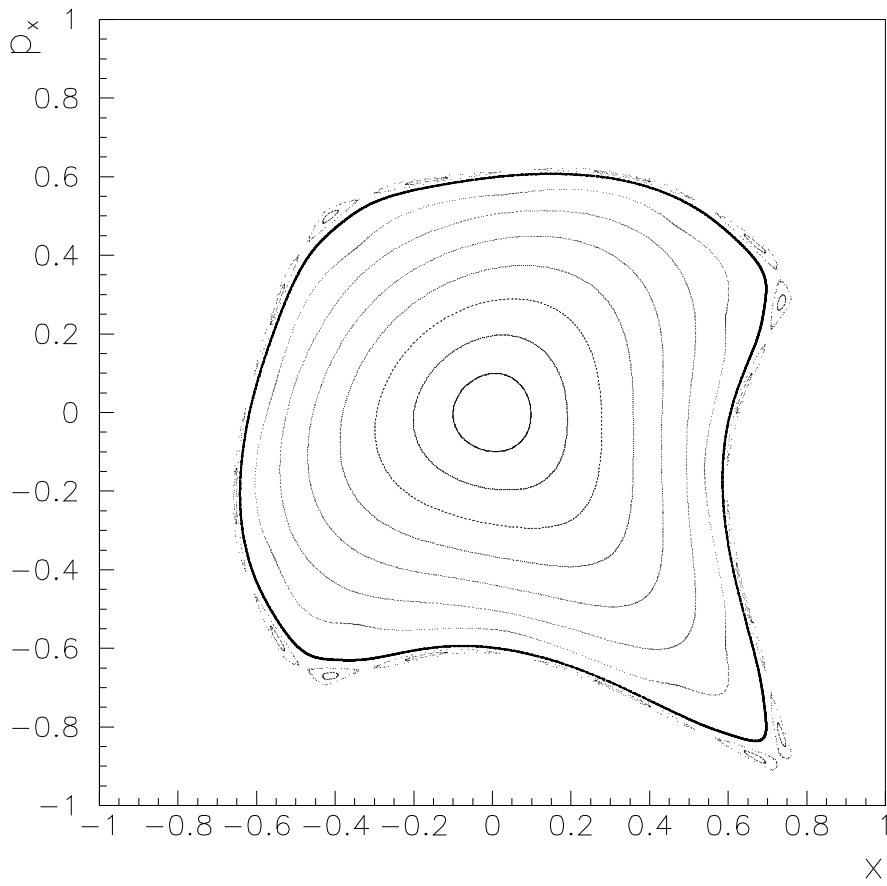
Figure 1: Phase portrait of the 2D Hénon map at $\nu = 0.28$. The last stable invariant connected curve is marked in boldface.
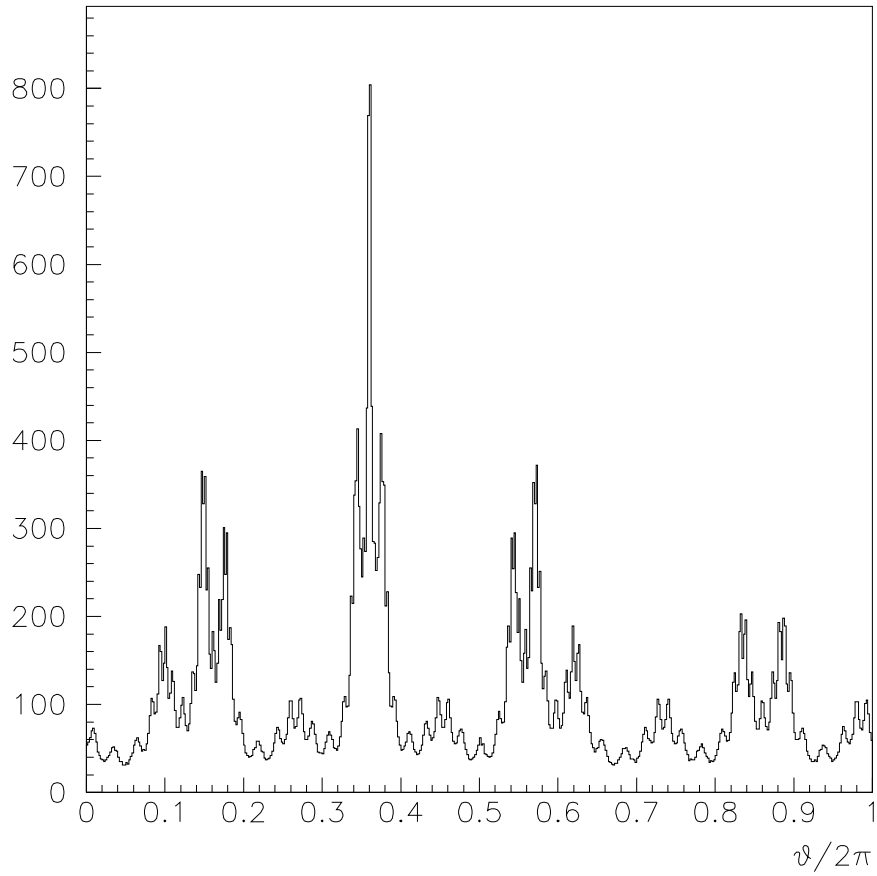
Figure 2: Distribution of the phases of the first 50000 iterates of the last stable invariant connected curve of the 2D Hénon map at $\nu = 0.28$.
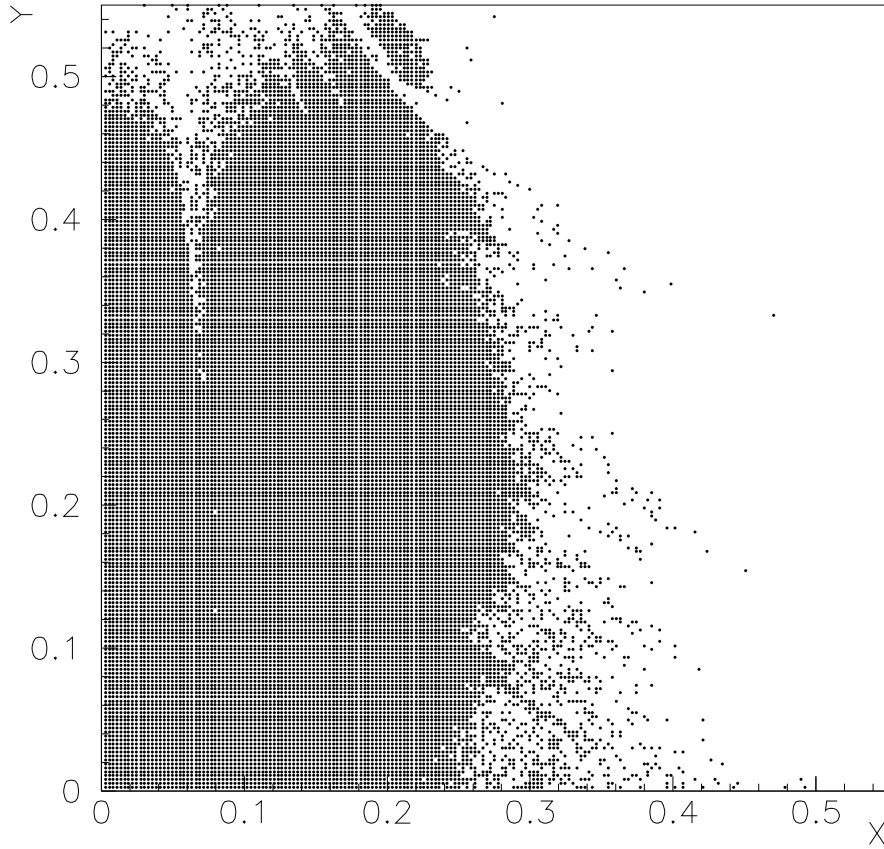
Figure 3: Stability diagram of the map (15) with $\mu = -0.2$, $\nu_x = 0.25$ and $\nu_y = 0.61803$; initial conditions which are stable up to 1000 iterations are plotted.
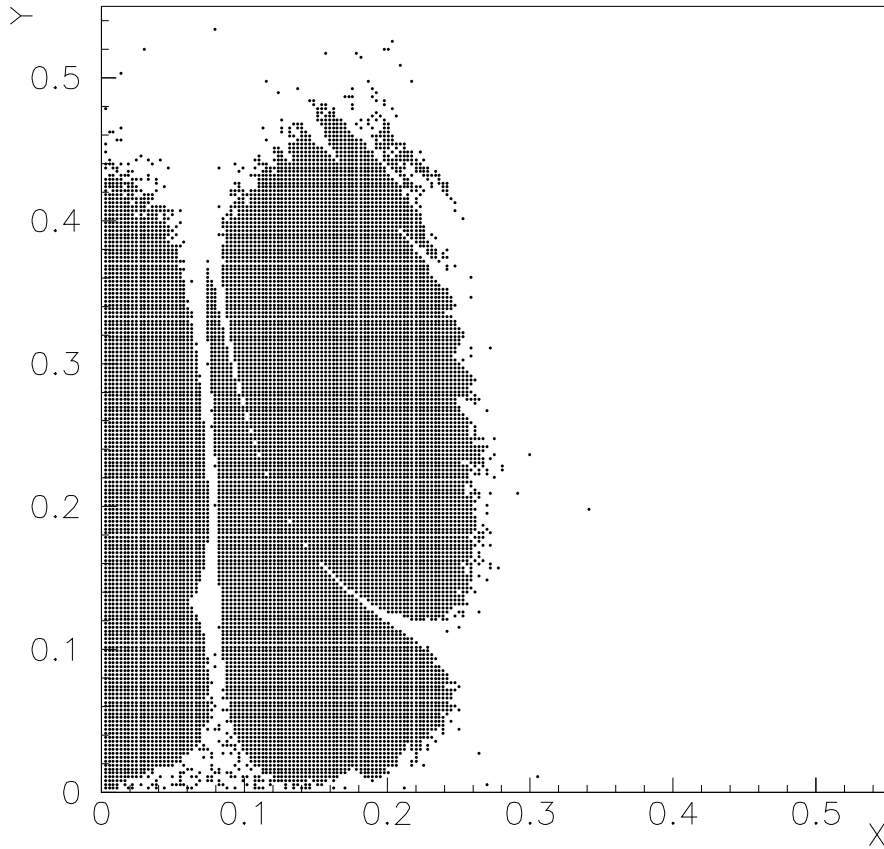
Figure 4: Stability diagram of the map (15) with $\mu = -0.2$, $\nu_x = 0.25$ and $\nu_y = 0.61803$; initial conditions which are stable up to 50000 iterations are plotted.
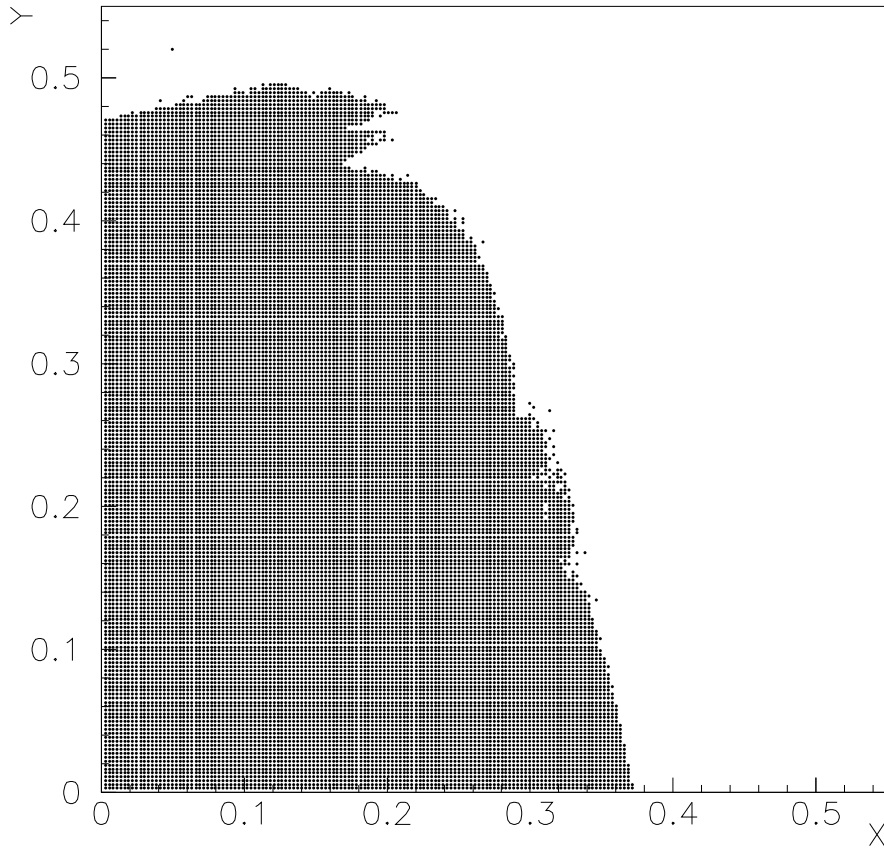
Figure 5: Stability diagram of the map (15) with $\mu = 1$, $\nu_x = 0.28$ and $\nu_y = 0.31$; initial conditions which are stable up to 1000 iterations are plotted.
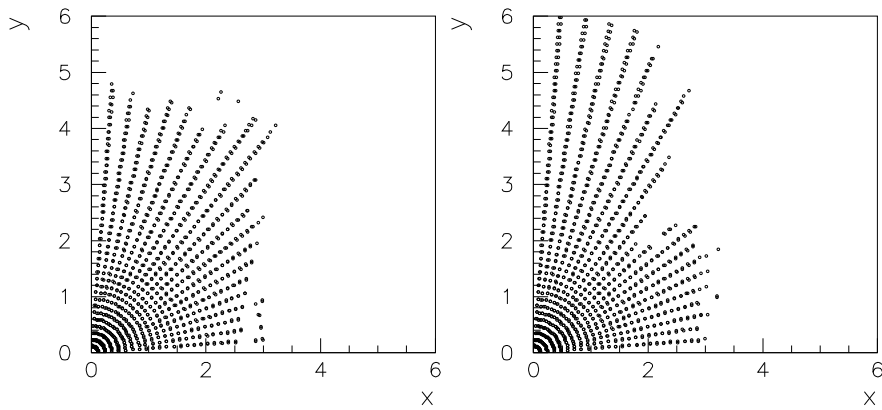
Figure 6: Stability diagram of the SPS with working point 1 (left) and working point 2 (right); initial conditions which are stable up to 1000 iterations are plotted.